Medical Physics
The International Journal of Medical Physics Research and Practice

In vivo measurements for high dose rate brachytherapy with optically stimulated luminescent dosimeters

Renu Sharma and Paul A. Jursinic

Citation: Medical Physics **40**, 071730 (2013); doi: 10.1118/1.4811143
View online: http://dx.doi.org/10.1118/1.4811143
View Table of Contents: http://scitation.aip.org/content/aapm/journal/medphys/40/7?ver=pdfcov
Published by the American Association of Physicists in Medicine

In vivo measurements for high dose rate brachytherapy with optically stimulated luminescent dosimeters

Renu Sharma[a] and Paul A. Jursinic
Department of Radiation Oncology, West Michigan Cancer Center, 200 North Park Street, Kalamazoo, Michigan 49007

(Received 2 April 2013; revised 30 May 2013; accepted for publication 31 May 2013; published 28 June 2013)

Purpose: To show the feasibility of clinical implementation of OSLDs for high dose-rate (HDR) *in vivo* dosimetry for gynecological and breast patients. To discuss how the OSLDs were characterized for an Ir-192 source, taking into account low gamma energy and high dose gradients. To describe differences caused by the dose calculation formalism of treatment planning systems.
Methods: OSLD irradiations were made using the GammaMedplus iX Ir-192 HDR, Varian Medical Systems, Milpitas, CA. BrachyVision versions 8.9 and 10.0, Varian Medical Systems, Milpitas, CA, were used for calculations. Version 8.9 used the TG-43 algorithm and version 10.0 used the Acuros algorithm. The OSLDs (InLight Nanodots) were characterized for Ir-192. Various phantoms were created to assess calculated and measured doses and the angular dependence and self-absorption of the Nanodots. Following successful phantom measurements, patient measurements for gynecological patients and breast cancer patients were made and compared to calculated doses.
Results: The OSLD sensitivity to Ir-192 compared to 6 MV is between 1.10 and 1.25, is unique to each detector, and changes with accumulated dose. The measured doses were compared to those predicted by the treatment planning system and found to be in agreement for the gynecological patients to within measurement uncertainty. The range of differences between the measured and Acuros calculated doses was −10%–14%. For the breast patients, there was a discrepancy of −4.4% to +6.5% between the measured and calculated doses at the skin surface when the Acuros algorithm was used. These differences were within experimental uncertainty due to (random) error in the location of the detector with respect to the treatment catheter.
Conclusions: OSLDs can be successfully used for HDR *in vivo* dosimetry. However, for the measurements to be meaningful one must account for the angular dependence, volume-averaging, and the greater sensitivity to Ir-192 gamma rays than to 6 MV x-rays if 6 MV x-rays were used for OSLD calibration. The limitations of the treatment planning algorithm must be understood, especially for surface dose measurements. Use of *in vivo* dosimetry for HDR brachytherapy treatments is feasible and has the potential to detect and prevent gross errors. *In vivo* HDR brachytherapy should be included as part of the QA for a HDR brachytherapy program. © *2013 American Association of Physicists in Medicine*. [http://dx.doi.org/10.1118/1.4811143]

Key words: optically stimulated luminescent dosimeters, high dose rate brachytherapy, *in vivo* dosimetry, Acuros algorithm

I. INTRODUCTION

One of the key responsibilities of a medical physicist is to implement a quality assurance program in the clinic. Such a program can include multiple, independent calculation checks and patient specific, *in vivo* dosimetry measurements[1–3] that confirm if the prescribed dose is correctly delivered to the patient.

To assure high accuracy in dose delivery from complex and conformal therapy-techniques, the AAPM TG-40 recommends[4] that clinics "should have access to thermoluminescent dosimeter (TLD) or other *in vivo* systems." *In vivo* dosimetry has been used extensively in external beam therapy, however its application to high dose-rate (HDR) brachytherapy has been limited.[5–8]

Thermoluminescent dosimeters and silicon diodes have been widely used for *in vivo* dosimetry. TLD dosimetry has been used for over 30 years and is a proven technology.[3,9–11] PN junction-type diodes[12,13] and metal-oxide–semiconductor field-effect transistors (MOSFETs; Refs. 14 and 15) have become very popular due to their immediate read out and high sensitivity; over 18 000 times that of an air filled ionization chamber of the same volume.[10,16,17] Plastic scintillation detectors[15,18] and Al_2O_3:C luminescent crystals[19–21] have been mounted on the end of fiber optic cables and have been used for brachytherapy measurements. These fiber optical systems have the capability of measuring dose delivery in real time.

Over the past couple of decades, synthetic materials that exhibit the property of thermally and optically stimulated luminescence, OSL, have been developed.[22,23] The most common OSL dosimeter material, α-Al_2O_3:C, has characteristics that make it a good *in vivo* dosimeter: 30–60 times the sensitivity to radiation as LiF:Mg,Ti TLDs;[24] read out can

be done optically;[25–29] and 2% signal fading[26] in the first 2.5 days.

In the past few years many papers have been published that describe the use of OSLDs in radiation oncology clinical measurements. This includes radiation delivered with heavy-ion beams[30,31] as well as photons, electrons, and protons.[26,28,32–35] In our clinic optically stimulated luminescent dosimeters, OSLDs, have been in use for a number of years and have been extended to HDR dosimetry.

The commercially available OSLD that is in clinical use is fabricated in a planar shape. How a planar detector, including an OSLD, responds to the incident angle of radiation will depend on the radiation field that is presented to the detector. The OSLD shows no significant angular dependence[26,36] when it is presented with high-energy x-rays in symmetric fields that occur in cylindrically symmetric phantoms. OSLDs show a 4% angular dependence[37] when irradiation is done in a moderately asymmetric-field that occurs in a rectangular phantom that has a 2:1 ratio of width-to-height. OSLDs show a 70% angular dependence[36] when irradiation is done in a highly asymmetric-field that occurs on the surface of a phantom. The angular dependence of an OSLD in a HDR radiation-field has not been previously investigated.

The response of InLight Dot OSLDs (Landauer, Inc., Glenwood, IL) to Ir-192 gamma rays has been characterized[26,31] but the OSLDs have not been used clinically. The InLight Dot was an early version of the OSLD that is no longer available. It has now been replaced by the Nanodot model OSLDs (Landauer, Inc., Glenwood, IL) that were used in this work. This work introduces the use of OSLDs for *in vivo* dosimetry measurements in patients being treated with HDR. High dose-gradients and low gamma energy are characteristics of HDR sources and these present unique requirements[38] for measurements: (1) detectors must have adequate spatial resolution to avoid volume averaging; (2) self-attenuation in a detector may be important; (3) dependence on the incident angle of radiation may be large; (4) energy dependence, and calibration for absolute dose are required. How to accommodate these requirements for OSLDs is presented along with clinical examples.

II. CALCULATION FORMALISM

If the radiation field varies across the disk of the Nanodot, then different portions of the Nanodot disk will receive different doses. Since the entire OSLD disk inside a Nanodot, see Fig. 1, is read at one time these different dose regions in the Nanodot disk will be read simultaneously and, thus, be averaged. So volume average of dose can occur. The dose distributions near HDR sources have high gradients and volume averaging by a Nanodot may be significant. Additionally, due to the higher effective atomic number of the OSLD compared to water there will be increased attenuation of fluence across the Nanodot compared to water.

To estimate the dose changes that can be expected in a Nanodot irradiated through its edge, the OSLD disk is divided into 11 columns of equal width. The use of 11 columns is chosen for practical not theoretical reasons: it adequately samples

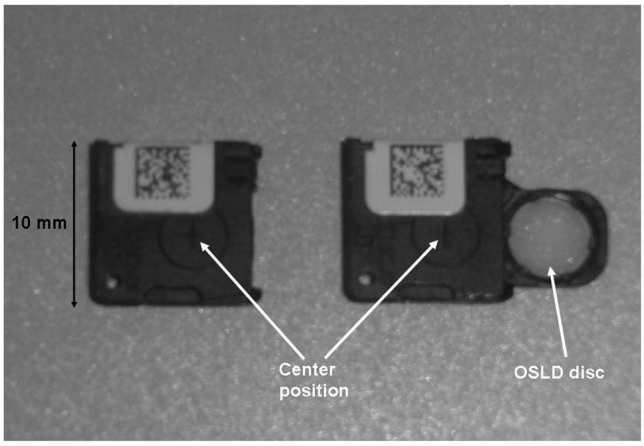

FIG. 1. A Nanodot with the OSLD disk in its light-tight case and with the disk pushed out from its case. The optical port with a 5-mm diameter that covers the OSLD disk can be seen. The position of the center of the OSLD disk and its optical port when it is in the case is shown as a "+" symbol on the outside of the case. Note that this center position is not in the center of the case but is offset by 1 mm in the longitudinal and lateral directions.

the change in dose across the OSLD disk and has one column that is centered in the middle of the disk. This segmentation scheme is shown in Fig. 2 and the characteristics of the segmented disk are shown in Table I.

The signal from reading the total disk is the following:

$$S_{total} = \sum_{i=1}^{11} S_i, \tag{1}$$

where S_i is the signal from each column,

$$S_i = K \times D_i \times A_i, \tag{2}$$

where K is a proportionality factor between dose and OSLD signal, D_i is the dose to the center of column i, and A_i is the area of column i.

If the dose is delivered from a point source to the left of the disk, as shown in Fig. 2, then the following holds:

$$D_i = D_{center} \times \left(\frac{l_{center}}{mid_i}\right)^2 \times T_i, \tag{3}$$

where D_{center} is the dose to the center of the disk if the Nanodot was water equivalent, l_{center} is the distance from the

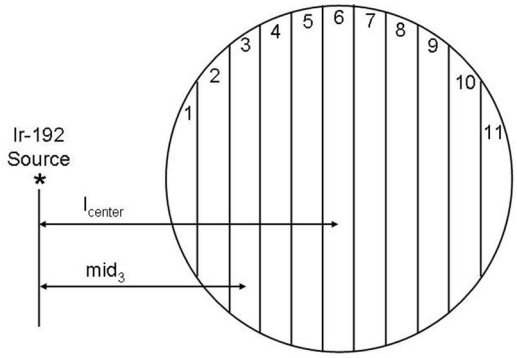

FIG. 2. A schematic of the segmentation into 11 columns that is used for calculation of attenuation and dose across a Nanodot disk.

TABLE I. Characteristics of a 5-mm diameter disk that is divided into 11 columns of equal width.

Column	Middle of the column, mid (mm)	Column left edge, le (mm)	Column right edge, re (mm)	Fraction of total area of the disk, A_i,[a]
1	0.23	− 2.50	− 2.05	0.045
2	0.68	− 2.05	− 1.59	0.079
3	1.14	− 1.59	− 1.14	0.097
4	1.59	− 1.14	− 0.68	0.108
5	2.05	− 0.68	− 0.23	0.114
6	2.50	− 0.23	0.23	0.116
7	2.95	0.23	0.68	0.114
8	3.41	0.68	1.14	0.108
9	3.86	1.14	1.59	0.097
10	4.32	1.59	2.05	0.079
11	4.77	2.05	2.50	0.045

[a] $A_i = \left(\frac{\pi r^2}{2}\right) \int_{le_i}^{re_i} \sqrt{r^2 + x^2}\,dx$

$A_i = \left[\frac{\pi r^2}{2}\right]\left[\left(\frac{re_i}{2}\right)\sqrt{r^2 + re_i^2} + \left(\frac{r^2}{2}\right)\sin^{-1}\left(\frac{re_i}{r}\right) - \left(\frac{le_i}{2}\right)\sqrt{r^2 + le_i^2} - \left(\frac{r^2}{2}\right)\sin^{-1}\left(\frac{le_i}{r}\right)\right].$

point source to the center of the disk, mid_i is the distance to the center of column i, and T_i is the transmission difference between any material and water. This transmission difference for the Nanodot case and the OSLD disk itself is the following[39]

$$T_i = \exp\left(- t_{ABS} \times \left(\left(\frac{\mu_{en}}{\rho}\right)_{ABS} \times \rho_{ABS} - \left(\frac{\mu_{en}}{\rho}\right)_{water} \times \rho_{water} \right) - t_{OSLD} \times \left(\left(\frac{\mu_{en}}{\rho}\right)_{OSLD} \times \rho_{OSLD} - \left(\frac{\mu_{en}}{\rho}\right)_{water} \times \rho_{water} \right) \right),$$

which reduces to

$$T_i = \exp\left(-t_{ABS} \times (\mu_{ABS} - \mu_{water}) - t_{OSLD} \times (\mu_{OSLD} - \mu_{water})\right). \quad (4)$$

Since $$t \times \left(\frac{\mu_{en}}{\rho}\right) \times \rho = t \times \mu,$$

where μ_{en}/ρ is the mass attenuation coefficient of the material, ρ is the mass density of the material, t is the thickness, and μ is the linear attenuation coefficient. μ_{ABS} is the linear attenuation-coefficient of the case material, t_{ABS} is the thickness of the case material, μ_{OSLD} is the linear attenuation-coefficient of the OSLD, and t_{OSLD} is the thickness of the OSLD, and μ_{water} is the linear attenuation-coefficient of solid water.

III. MATERIAL AND METHODS

OSLD irradiations were made using the GammaMedplus iX Ir-192 HDR (Varian Medical Systems, Milpitas, CA). The air kerma strength of the source was measured with a model HDR100Plus well chamber (Standard Imaging, Middleton, WI) that had been calibrated at the University of Wisconsin Dosimetry Calibration Laboratory an Accredited Dosimetry Calibration Laboratory.

Patient and phantom CT scans were done with a Philips Big-bore machine (Philips Electronics North America Corporation, Andover, MA). For HDR patients the scan technique used was 120 KV, 50 mA, and helical scans with slice thickness of 3 mm.

The x-ray beam used in this work had nominal energy of 6 MV. For this energy the percentage depth-dose of x-rays at depth of 10 cm, %dd(10), was 66.6, which was measured at the source-to-surface distance, SSD, of 100 cm, according to the TG-51 protocol.[40] The radiation beams were generated by a Varian Trilogy Linear Accelerator (Varian Medical Systems, Milpitas, CA). Absolute dose measurements were made with a cylindrical ion-chamber, model N30001 (PTW Freiburg Germany), which was calibrated at the University of Wisconsin Dosimetry Calibration Laboratory. In our clinic the calibrated output is adjusted to be 1 cGy = 1 MU to water with a 10 × 10-cm field, source-to-detector distance of 100 cm, with the detector at a depth of maximum dose. The Nanodots were calibrated with this x-ray beam as previously published.[26]

The OSL dosimeters used in this study were InLight Nanodots (Landauer, Inc., Glenwood, IL) shown in Fig. 1. The OSLDs have a 5-mm diameter, are 0.2-mm-thick, plastic disk infused with aluminum oxide doped with carbon (Al_2O_3:C, synthetic sapphire), with front-and-back, 0.05-mm thick, polyester-film, cover layers. These disks are encased in a light-tight plastic holder made of Acrylonitrile butadiene styrene, ABS, and the holder is 0.085 mm thick. As shown in Fig. 1, the OSLD disk is asymmetrically located; 1-mm off center, in the plastic case of the Nanodot. From an edge-on direction the radiation passes through 3.5 or 1.5-mm thickness of the ABS holder, which depends on the edge through which the radiation enters.

OSLDs were read with an InLight MicroStar reader (Landauer, Inc., Glenwood, IL). This reader operates in continuous-wave, cw, mode with a 1-s illumination read-period. In cw mode the read-light intensity is constant for the read period. The reader was operated in its "hardware test" modality, using the low-intensity LED-beam for preirradiation and postirradiation measurements. This allowed repeated readings of an OSLD with a signal decrease per reading of 0.05%.[26] Three readings are made of an OSLD and averaged with no correction made for the 0.15% reading depletion. All of the OSLD readings in this work, including calibrations, were corrected for changes in the intensity of the reading light. A reading is determined as follows:

$$R = (OSLD - Count)/LED, \quad (5)$$

where OSLD-count is the OSLD signal and LED is the LED signal that is determined when the OSLD is read.

The LED light intensity was monitored with the LED function of the reader, which was modified to give about 48 000 counts for the LED test. This gave an uncertainty in the measurement of the light intensity of $1/\sqrt{48\,000} = 0.0046$ based on count statistics.

New Nanodots that had only received a few hundred centigray and "linearized" Nanodots were used in accordance with previously published protocols.[26,34,35] The linearized Nanodots were preirradiated with 2 kGy or more, which linearized their response to dose.[34] The detectors were used repeatedly and were optically reset after each exposure. The optical reset method, as previously described,[34] uses a bright white, 14 W, compact fluorescent lamp, CFL. In this work the UV content of the CFL was reduced by shielding the Nanodots with a F007-004 UV filter (UV Process Supply, Chicago, IL). The readings were made between 8 and 60 min following an irradiation to allow the transient signal to decay and to avoid signal fading, respectively. The dose was calculated as follows:

$$D = S \times (R_a - R_b), \tag{6}$$

where S is the dose sensitivity of the Nanodot, R_b is the reading immediately before the irradiation, and R_a is the reading after the irradiation. R_b must be established before each irradiation since the background signal slowly changes[26,34] during storage in the dark. S is established by irradiating the Nanodot with 20 cGy of 6 MV x-rays[35] and reading its response. After each dose measurement, the Nanodot is optically reset and a current S value is established for each Nanodot.

Measurement of the linear attenuation-coefficients of various materials was done with a surface diode, model SI4 (Ref. 41) (Standard Imaging, Madison, WI). The diode output was measured with a Max4000 electrometer (Standard Imaging, Madison, WI) operated in the zero-bias mode. The diode and HDR catheter were mounted on a block of high-density Styrofoam, mass density 0.033 g/cm^3, and were separated from each other by the 7.5-cm block thickness. Various thicknesses of 7-mm diameter disks of the material to be measured were placed directly over the HDR catheter in a cavity cut into the Styrofoam block. This geometry is used to measure the broad-beam mass attenuation-coefficient.[9]

A variety of phantoms were used for measurements in this work. When measuring on the surface of a HDR vaginal-cylinder applicator, the Nanodot was taped to the outside of the 30-mm diameter cylinder. The cylinder-Nanodot combination was wrapped with concentric layers of Superflab, a flexible water-equivalent material (Civco, Orange City, IA) to give a final diameter of 20 cm. Additional Nanodots were placed in the layers of Superflab at desired distances from the cylinder surface.

Measurements of angular dependence of Nanodots were made with the apparatus shown in Fig. 3, which was constructed with solid water (Standard Imaging, Middleton, WI). The Ir-192 source and the detectors were separated by 9.5-cm thick stack of solid water. As shown in Fig. 4, the OSLD is held in a slot at the end of a 16.5-mm diameter cylindrical-

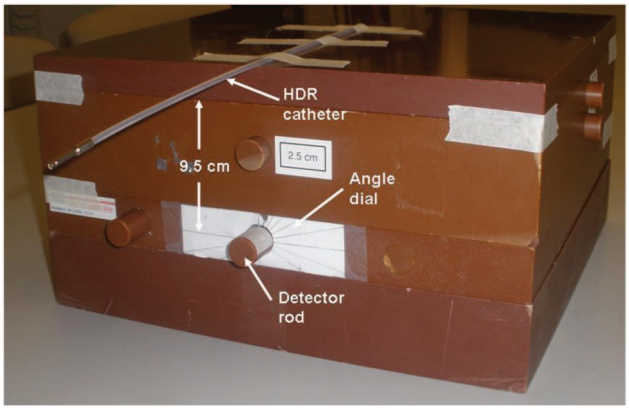

FIG. 3. The test apparatus for angular dependence that was assembled with slabs of solid water. The position of the HDR catheter and a dial for setting the angle of the face of the Nanodot with respect to the HDR source are shown.

rod that is machined to fit snuggly in the solid water slab. The OSLD case is mounted asymmetrically with the center of the detector volume being collinear with the cylindrical axis of the rod. The residual volume of the slot was filled with M3,[42] a water equivalent material.

Measurements of Nanodot dependence on dose rate were done in air away from large objects that scattered dose. To accomplish this, a 3-m long cotton string was pulled and tightened with at least 1.5-m distance between it and the walls and floor of the shielded room. An Ir-192 plastic catheter and Nanodot were secured on the string at measured distances from one another. The dose rate at the position of the detector was calculated according to the following equation in TG-43,[43] which has been simplified for a point source in air:

$$\dot{D}(r) = S_k \Lambda / r^2, \tag{7}$$

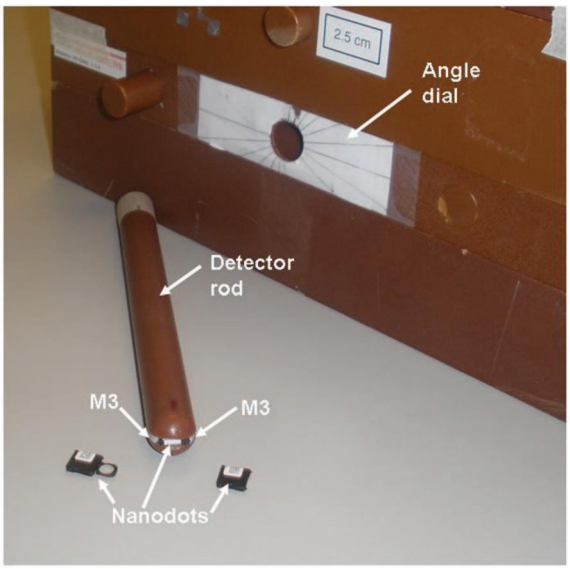

FIG. 4. The rod that holds the Nanodot in the desired angular position. M3 is water-equivalent material used to fill the gap in the slot.

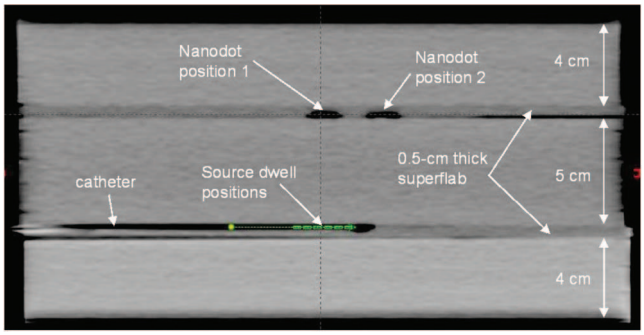

FIG. 5. A CT image of the test apparatus that was assembled from slabs of solid water and pieces of 0.5-cm thick Superflab. Shown in the image are the locations of the HDR catheter, six dwell locations that are used, and two Nanodots.

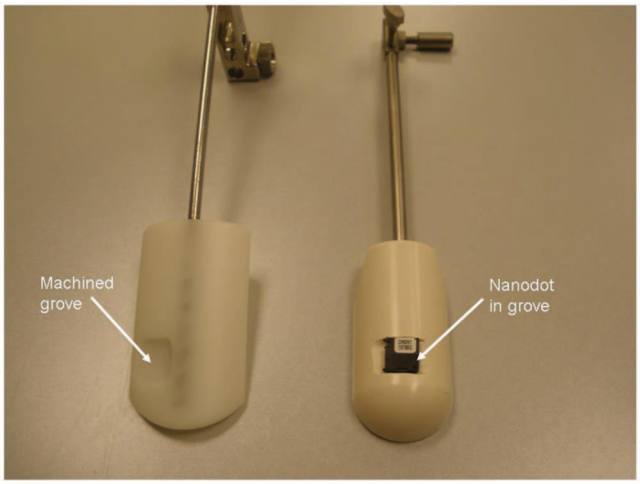

FIG. 6. Rectal retractors from HDR gynecological applicator-sets. These retractors have been modified by having a grove milled into the plastic that can hold a Nanodot.

where $\dot{D}(r)$ is the dose rate at distance r from the source, S_k is the air kerma strength, and Λ is the dose rate constant.

For general measurements of dose, solid-water slabs are used as shown in Fig. 5. In this case, the distance between the source and the detectors is maintained at 5.25-cm; 5.0 cm of solid water, plus half of the 3-mm diameter of the catheter, and half of the 2-mm thickness of the Nanodot case. The use of Superflab avoided the need for the slabs of solid water to be machined for the various detectors. The Superflab and solid water were used for buildup and backscatter material. The material thickness above the Nanodots in Fig. 5, 0.5-cm Superflab and 4-cm of solid water, can be changed to alter the scatter environment adjacent to the Nanodot.

It has been reported[44] that the relative fluence of low energy photons increases with distance from an Ir-192 source. To test if Nanodot sensitivity might be affected by changes in the separation distance in solid water, a phantom arrangement similar to Fig. 5 was used. For these measurements the thickness of buildup material above the Ir-192 catheter and the detector was kept at 10 cm and the separation distance between the source and the detector was varied. Also, a single dwell position was used that was centered over the detector. For comparison purposes dose was measured with a parallel-plate ion chamber, model N23343 (PTW Freiburg Germany). A slab of solid water was used that was machined to hold the parallel plate chamber.

InLight Dot response to Ir-192 gamma rays has been shown in Refs. 26 and 31 to be 5%–9% higher than to 6 MV x-rays. This difference in response Ir-192 gamma rays and 6 MV x-rays is due to the OSLD composition being different than water. For LiF:Mg,Ti thermoluminescent dosimeters that have been calibrated with MV x-rays, it is recommended[43] that no correction be made for changes in sensitivity for low energy gamma rays from brachytherapy sources. Recent work[45] has shown that TLDs have an over response of 5% at Ir-192 gamma energy compared to MV x-rays and it is recommended that corrections should be made. In this work Nanodot and linearized Nanodot sensitivity to Ir-192 gammas is measured and compared to the sensitivity to 6 MV x-rays. These measurements were done as previously published[26] in solid water with a 7.1-cm separation between the Ir-192 source and the detector with full backscatter. The dose at the detector position was calculated with the BrachyVision software.

For Nanodot measurements in cervical cancer patients, the rectal retractors were modified as shown in Fig. 6. The Nanodot was positioned in the machined groove and the retractor was then covered with the stretched thumb of a latex surgical glove that was taped to the metal rod of the retractor. The latex sleeve ensured that the detector was kept clean and dry and mitigated the chance of detector migration or loss.

Measurements were made on the skin surface of the breast for patients that were treated with accelerated partial breast irradiation (APBI).[46] As shown in Fig. 7, five Nanodots were placed on the patient's skin in a square configuration with Nanodots in the middle and at the corners of the square. The corner positions were 1.5 cm from the middle position. The middle position was placed over the center of the catheter and the corner positions were superior, inferior, left, and right of the center. This pattern of detectors is used since the precise

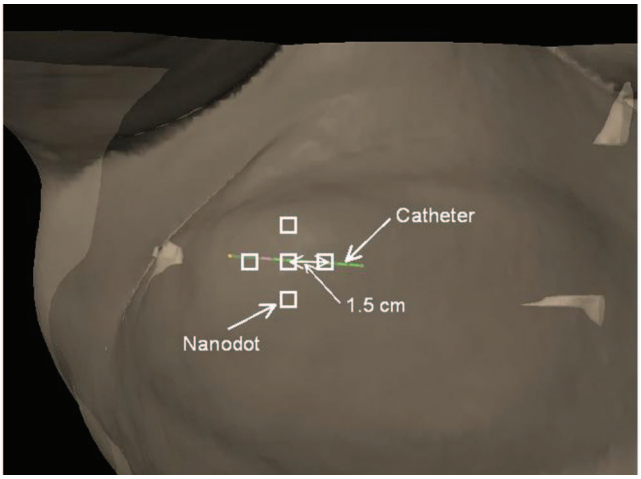

FIG. 7. The geometric arrangement of Nanodots placed on the surface of the breast when making a measurement of surface dose.

location on the skin surface above the HDR catheter is difficult to determine.

All treatment plans were generated with BrachyVision, versions 8.9 and 10.0 (Varian Medical Systems, Milpitas, CA). Version 8.9 used the TG-43 algorithm[47] and version 10.0 used the Acuros algorithm.[48–52] The TG-43 calculation algorithm does not correct for tissue inhomogeneity and presumes an infinite extent of water-equivalent material. The Acuros algorithm is based on the explicit solution of the Linear Boltzmann transport equation versus the stochastic solution of Monte Carlo-based methods. The Acuros algorithm is a model-based dose calculation method that has been characterized as a grid-based Boltzmann equation solver.[53] Acuros corrects for tissue inhomogeneity both in beam attenuation and dose deposition and recognizes the patient surface and all internal structures and contours. Values for tissue heterogeneity and applicators were obtained from their CT electron density values and were not manually overridden. The resolution of the calculation grid was 2.5 mm and dose was calculated to the local tissue composing each voxel not to water. The 2.5-mm calculation grid resolution is used in patient calculations and was chosen to maintain short calculation times. A number of calculations were carried out with 1-mm resolution and point doses were found to be altered by 0.5% or less in all cases.

IV. RESULTS

The sensitivity of Nanodots that are new, used for three months, and linearized to Ir-192 photons was measured as previously described.[26] These results are shown in Table II. It is clear that the OSLD response to Ir-192 versus 6 MV x-rays depends on the type of detector. New InLight Nanodots have a 4% higher response than the InLight Dot that was available five years ago. The differential response also depends on the dose history of the device. The linearized Nanodot, which has received more than 2 KGy, has a 15% higher response than the new Nanodot, which had received only 0.02 Gy. Nanodots that had been used for three months and had gone through 8 cycles of irradiation and zeroing and received about 15 Gy have a 13% higher response than the new Nanodot. In this work the appropriate Ir-192 sensitivity factor in Table II is applied to dose measurements.

Many detectors show a dependence on dose rate. This was checked for Nanodots by measuring dose at different distances from the source. As shown in Eq. (7), the dose rate will fall with the square of the separation distance. The delivered dose was kept constant by keeping the irradiation time/distance^2 constant. The results of this experiment are shown in Fig. 8. Within experimental uncertainty, the sensitivity of the Nanodot does not change from a distance in air of 2–10 cm away from the Ir-192 source. This corresponds to a change in dose rate of 3.5–0.14 cGy/s at 2 and 10 cm, respectively.

TABLE II. The ratio of various OSLD's sensitivity to Ir-192, S(Ir-192), and the 6 MV x-rays, S(6 MV) is shown. For these measurements the separation of the Ir-192 source from the detectors is 7.1 cm of solid water. The number of measurements, n, that were made is indicated and the error indicates one standard deviation. The Dot detector data are from Fig. 10 of Ref. 26.

Detector	S(Ir-192)/S(6 MV)
Nanodot, new ($n = 5$)	1.10 ± 0.005
Nanodot, used for 3 months ($n = 11$)	1.23 ± 0.025
Nanodot, linearized ($n = 5$)	1.25 ± 0.020
Dot, new	1.06 ± 0.015

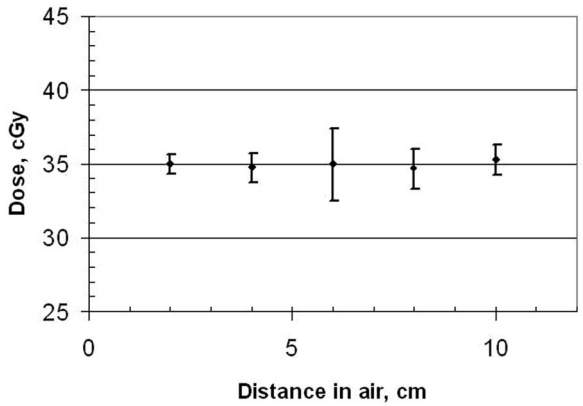

FIG. 8. The measured dose at various distances in air away from the Ir-192 source. The dose rate is 3.5 cGy/s at 2 cm and the irradiation time is 10 s for a delivered dose at the position of the detector of 35 cGy. The dose rate decreases by 1/distance^2 and the delivered dose is kept constant by increasing the irradiation time by distance.^{2} Typical error bars for one standard deviation are shown. These standard deviations are based on four repeats of the experiment.

To test if Nanodots sensitivity might be affected by changes in the separation distance in solid water, a phantom arrangement similar to Fig. 5 was used. Different separation distances were accomplished by adding slabs of solid water. The dose was measured with Nanodots and by a parallel-plate ion chamber imbedded in a slab of solid water. The delivered dose was kept approximately the same by keeping the irradiation time/distance^2 constant. The results are shown in Fig. 9. From a separation distance of 1–10 cm of solid water the relative Nanodot sensitivity increase by about 10%, which is greater than experimental uncertainty.

Figure 9 shows the combined error of Nanodot and ion chamber readings. The error in a Nanodot measurement under controlled geometry of a depth of 3 cm was determined by making measurements with five separately calibrated Nanodots. The average measurement was 63.5 cGy with one standard deviation of 1.0 cGy or a coefficient of variation of 1.5%. Using the same geometry, five ion chamber measurements were found to have a coefficient of variation of 0.4%.

Measurements of the attenuation of ABS, OSLD disks, and solid water are shown in Fig. 10. The data are fit by an exponential equation and give the following linear attenuation coefficients: $\mu_{ABS} = 0.0195 \pm 0.0011$ mm^{-1}, $\mu_{OSLD} = 0.0150 \pm 0.0016$ mm^{-1}, and $\mu_{water} = 0.0100 \pm 0.0005$ mm^{-1}.

These attenuation data and the parameters in Table I are applied to Eqs. (1)–(4) to calculate the expected difference in Nanodot signal if the source is facing the edge or the front of the Nanodot. For the front surface, $t_{ABS} = 0.051$ mm and

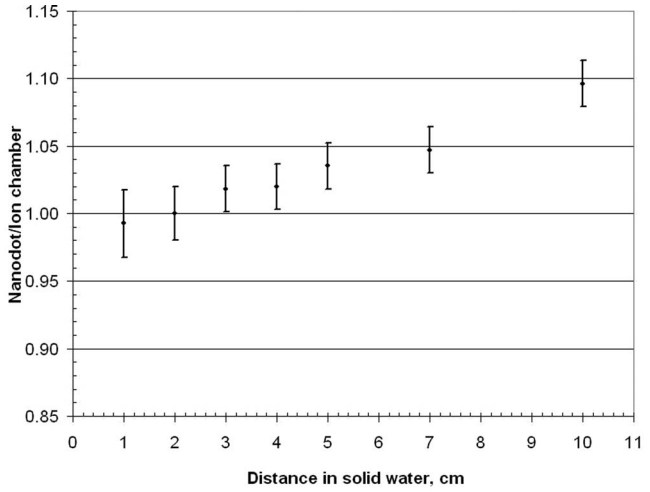

FIG. 9. The ratio of Nanodot to ion chamber measured dose at various distances in solid water away from the Ir-192 source. The ratio is normalized at a distance in solid water of 2 cm. The dose rate is 5 cGy/s at 1 cm and the irradiation time is 8 s for a delivered dose at the position of the detector of 40 cGy. Typical error bars for one standard deviation are shown. These standard deviations are based on four repeats of the experiment.

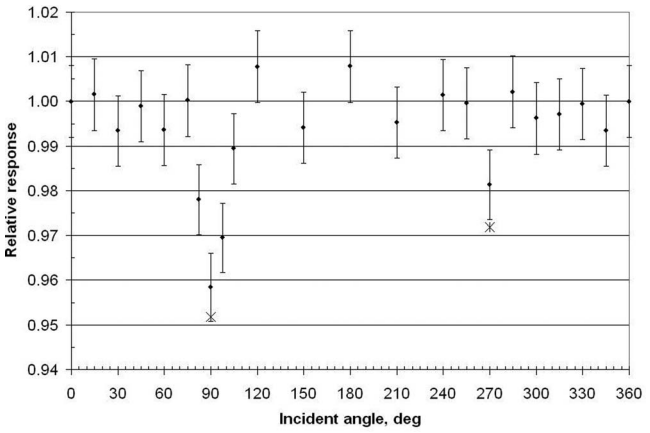

FIG. 11. Measurement of the dependence of Nanodot sensitivity on the incident angle of Ir-192 gamma rays. The experimental setup is shown in Figs. 3 and 4. The incident angle of 0° corresponds to the front surface, 90° to the thick edge of the Nanodot, and 270° to the thin edge of the Nanodot. Typical error bars for one standard deviation are shown. These standard deviations are based on four repeats of the experiment. The asterisks are calculated responses based on attenuation through the Nanodot as explained in the text.

$t_{OSLD} = 0.085$ mm. The calculated ratio of signal from the edge and from the front is 0.953 for the 3.5-mm thick edge and 0.973 for the 1.5-mm thick edge. These values are indicated by asterisks in Fig. 11, which shows the Nanodot sensitivity to the direction of angular incidence of Ir-192 gamma rays.

The comparison of the Nanodot measurement of dose and the calculation of dose in a known geometry, Fig. 5, was done. The treatment plan used 5-dwell positions, 5 mm step-size with a prescribed dose of 284 cGy to position 1 and 221.0 cGy to position 2. The measured and calculated dose for different thickness of material above the Nanodots is shown in Fig. 12. The maximum dose gradient was determined from the calculated dose distribution to be 12 cGy/mm for point 1 and 7 cGy/mm for point 2. The error in the position of the detector with respect to the source position is estimated to be ±1 mm based on the location of the detector in the CT of the phantom determined by two independent clinicians. This position uncertainty corresponds to an uncertainty in calculated dose of 12 cGy for point 1 and 7 cGy for point 2 and is depicted by the error bars in Fig. 12. The dose calculated with the TG-43 algorithm does not change with the material thickness because the treatment planning system presumes that an infinite extent of water-equivalent material exists regardless of the actual geometry. The measured dose reaches a maximum when thickness of the backscatter material is 4.5 cm. The measured dose is 11%–15% lower with no added material; which is equivalent to a dose measurement at the surface. The dose calculated with the Acuros algorithm predicts the rise in the measured dose with increased thickness of buildup material. The nominal delivery time for this plan was

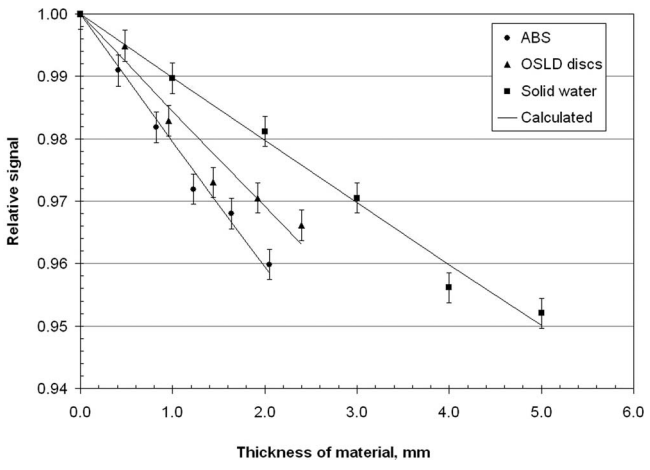

FIG. 10. Measurement of the attenuation coefficient of various materials to Ir-192 gamma rays. Typical error bars for one standard deviation are shown. These standard deviations are based on four repeats of the experiment. The solid lines are exponential fits to the data.

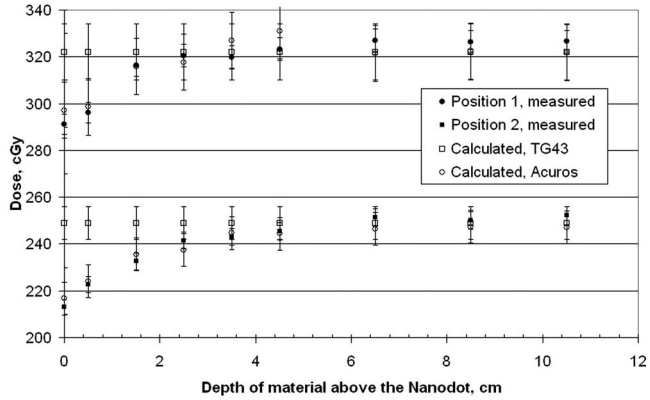

FIG. 12. Measurement of dose with various amounts of solid water and superflab above the linearized Nanodot. The experimental setup is shown in Fig. 5. For the measured points, typical error bars for one standard deviation are shown. These standard deviations are based on four repeats of the experiment. The calculated data are from the TG-43 and Acuros algorithms. The error bars on these calculated data correspond to ±1 mm in the location of the dose point.

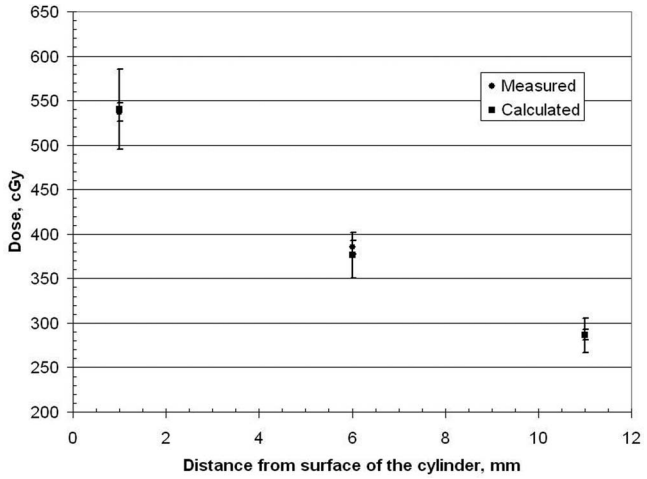

FIG. 13. Measurement of dose at different positions around a vaginal cylinder wrapped with Superflab. The distance from the surface of the cylinder is to the middle of the Nanodot disk. In these measurements linearized Nanodots were used. Typical error bars for one standard deviation are shown. These standard deviations are based on four repeats of the experiment. The error bars on these calculated data correspond to ±1 mm in the location of the dose point.

636 s, which is a dose rate of 284 cGy/636s = 0.45 cGy/s at position 1. This dose rate will vary with source strength and measurement position but 0.5 cGy/s is a typical value found in measurements done in our clinic for an Ir-192 source with 10 Ci activity.

Measurements of dose around the vaginal cylinder are shown in Fig. 13. The dose gradient at the three distances from the cylinder surface was determined from the calculated dose distribution to be 45, 26, and 19 cGy/mm at distances of 1, 6, and 11 mm, respectively. The error in the position of the detector with respect to the source position is estimated to be ±1 mm, which corresponds to an uncertainty in calculated dose of 45, 26, and 19 cGy, at distances of 1, 6, and 11 mm, respectively. The error bars in Fig. 13 depict these uncertainties. The measured doses are found to be in agreement with the doses calculated with the TG-43 algorithm. This is expected since the depth of material above the detector is at least 7.5 cm, which is adequate for full buildup of dose as shown in Fig. 12.

This experimental apparatus was also imaged with CT and radiographic procedures used on HDR patients. The Nanodot signals from these imaging procedures had counts that corresponded to less than 2-cGy of Ir-192 dose. Consequently, no correction was made for dose deposited by CT scans.

Measurements were made on the rectal retractors for three tandem and ring patients. Seventeen measurements were made and these data are shown in Table III. Five tandem and ovoid patients were measured on multiple fractions. The measurements were compared to calculations made with the TG-43 and Acuros algorithms. The differences were in a range from +13.7% to −14.9%. It is also of interest that the TG-43 and Acuros calculations of dose are very similar. The ratio of Acuros dose to TG-43 dose is 0.97 with a coefficient of variation of 2%. This close agreement in these calculations of dose is expected since in the position of the rectal retractor there is adequate buildup material and small amount of tissue heterogeneity.

TABLE III. Measurements made with a Nanodot mounted on a rectal retractor versus the dose calculated with the TG-43 and Acuros algorithms. The average distance between the sources and the Nanodot is 3 cm so the S(Ir-192)/S(6 MV) ratio used is 1.25/1.03 = 1.21 based data in Table II for a linearized Nanodot and Fig. 8. The percent difference is 100(measured-calculated)/calculated.

Measurement	Measured dose (cGy)	TG-43 calculated dose (cGy)	Acuros calculated dose (cGy)	TG-43 difference (%)	Acuros difference (%)	Maximum dose gradient (CGy/mm)	Maximum dose gradient (%/mm)
1	212	213	207	−0.4	2.5	17.8	8.6
2	203	209	211	−2.7	−3.6	14.1	6.7
3	183	164	161	11.6	13.7	10.6	6.6
4	212	232	225	−8.5	−5.7	11.7	5.2
5	215	227	217	−5.3	−1.0	12.4	5.7
6	204	213	203	−4.1	0.6	11.6	5.7
7	204	226	216	−9.6	−5.4	12.1	5.6
8	180	196	187	−8.0	−3.5	4.9	5.9
9	188	205	197	−8.1	−4.4	11.6	5.9
10	126	139	133	−9.7	−5.6	7.7	5.8
11	192	203	194	−5.5	−1.1	12.4	6.4
12	175	194	188	−9.7	−6.9	10.1	5.4
13	174	176	173	−1.0	0.7	10.9	6.3
14	141	140	140	1.1	1.1	8.7	6.2
15	183	170	172	7.7	6.4	13.0	7.6
16	163	172	169	−5.4	−3.7	13.0	7.7
17	156	166	164	−6.2	−5.1	11.6	7.1
18	256	263	251	−2.8	1.8	15.2	6.0
19	157	185	175	−14.9	−10.1	10.1	5.8
20	192	188	189	2.1	1.5	13.8	7.3

TABLE IV. Measurements and calculations for dose on the skin of the breast for positions at and around the center of the catheter. The measured value shown is the maximum of the five Nanodots placed on the patient. The average distance between the sources and the Nanodot is 2.5 cm so the S(Ir-192)/S(6 MV) ratio used is 1.25 × 0.85/(1.04) = 1.02 based data in Table II for a linearized Nanodot and Figs. 9 and 12. The percent difference is 100(measured-calculated)/calculated.

Patient	Measured dose (cGy)	TG-43 calculated (cGy)	Acuros calculated dose (cGy)	% diff measured (Acuros)	Maximum dose gradient (cGy/mm)	Maximum dose gradient (%/mm)
1	426	431	400	+6.5	11.5	2.9
2	407	458	426	−4.4	32.0	7.5
3	293	321	291	+0.7	15.5	5.3

The position of the detector was located in the CT images of the patient by two independent clinicians. The vector distance of the difference in these locations was from 0.4 to 3.2 mm with an average of 1 mm. Based on the average dose gradient shown in Table III, 12 cGy/mm, this corresponds to 5–39 cGy or a range of 2%–18% in calculated dose. Based on this analysis the differences between measured and calculated dose are due to uncertainty in locating the position of the detector with respect to the HDR source dwell positions in the CT image.

Measurements were made on the skin surface of the APBI patients. These patients were treated with a single-catheter balloon applicator that is about 2.5 cm below the skin and guides the HDR Ir-192 source. The skin surface dose for these patients should not exceed 425 cGy or 125% of the prescribed dose. Morbidity is associated with high dose on the skin surface for this type of treatment.[54] Data for three patients are shown in Table IV. No correction was made for angular dependence since the angle of the line from the source to the detector will be less than or equal to arctan(1.5/2.5) = 31°. Based on the data in Fig. 11, within experimental uncertainty there will be no need for an angular correction. As expected from the results shown in Fig. 12 the dose calculated with the TG-43 algorithm is about 8%–10% higher than the Acuros calculation of dose. This difference is due to the TG-43 calculation algorithm assumption of a phantom of infinite extent even though the detector is on the skin surface. The measured dose is −4.4% to +6.5% of the Acuros calculated dose. Based on the dose gradient shown in Table IV this is consistent with the distance between the detector and the source location being 0.1–2.2 mm of what is observed on the CT image. Since the patient is moved from the CT couch to the treatment couch a 2 mm change in the position of the skin surface of the breast with respect to the source applicator is possible.

V. DISCUSSION

In vivo dosimetry measurements in HDR treatments occur in an environment with high dose-gradients and low gamma energy. This requires a detector that meets demanding requirements[38] for measurements. How OSLDs can be used for HDR measurements is now discussed.

A detector must have adequate spatial resolution to avoid volume averaging. The highest dose-gradient at the position of a rectal retractor in a tandem and ring plan is 12 cGy/mm. The rectal dose is typically 200 cGy, so to have less than 1% change in dose, 2 cGy, a detector must have dimensions less than 0.2 mm (2 cGy/12 cGy/mm). This only occurs with a Nanodot if it is irradiated on the front or back faces. The cross dimension of a Nanodot is 5-mm, so when irradiated through an edge of a Nanodot does not meet this 1% requirement. The Nanodot will suffer a volume averaging problem if irradiated through an edge.

The self-attenuation of the Nanodot disk and attenuation of its case have been quantified in Figs. 10 and 11. Making a simple calculation of the difference in attenuation of Nanodot materials and water for Ir-192 gamma rays, one predicts an angular dependence. Irradiation through the edge of the Nanodot is expected to give a lower signal than a face-on direction. Also, one edge of the case is thicker than the other and the lowest signal will occur for irradiation through the thick edge. This behavior is found experimentally and is shown in Fig. 11 where 90° is the thick edge versus 270° is the thin edge.

The combination of volume averaging and attenuation gives rise to a dependence on the incident angle of radiation. In order to avoid correction factors it is best to place the Nanodot so that the Ir-192 source is orthogonal to the face of the detector.

The InLight Dot OSLD response to Ir-192 gamma rays has been shown[26,31] to be 5%–9% higher than to 6 MV x-rays. In this work, a sensitivity factor of 1.10, Ir-192 gamma to 6 MV x-rays, is found for new Nanodots that had received only 20 cGy of dose. However, as shown in Table II the Ir-192 sensitivity factor depends on the type of OSLD as well as the dose history of the OSLD. Based on these results it is recommended that Nanodots that are going to be used for Ir-192 measurements be calibrated with 20 cGy of dose from Ir-192 not from 6 MV x-rays. This will avoid the uncertainty in the different sensitivity of OSLDs to Ir-192 gammas versus 6 MV x-rays. Calibration of Nanodots with 6 MV x-rays and presuming that the sensitivity ratio is constant introduces an avoidable error.

Many detectors show a dependence on dose rate when the dose rate under measurement conditions is much higher than in calibration conditions. This was investigated for OSLDs in earlier work.[26] It was shown that no dose-rate dependence occurred in OSLDs for dose rates in the range of

23–9560-cGy/s. The dose rates in this work and most HDR clinical situations are about 0.5-cGy/s, which is well below previously tested dose rates. As expected, it is shown in Fig. 8 that no dependence on dose rate is seen for Nanodots at dose rates that are found in HDR treatments.

The average photon energy around an Ir-192 point source has been reported[44] to decrease from 337 keV at 1 cm to 221 keV at 10 cm from the source in water. With such a decrease in photon energy one would expect the OSLD sensitivity to increase with distance away from the source based on the energy dependence shown by Reft.[31] This is confirmed in Fig. 9 as a 10% increase in sensitivity when measured at 10 versus 1 cm from the Ir-192 source. It is interesting that a much larger change in sensitivity of 25% has been reported[55] for MOSFET measurements made at 1 versus 5 cm from an Ir-192 source.

In vivo measurements of dose at the rectal surface of gynecological cancer patients were found to be within the uncertainty of the calculated dose. Nevertheless, the OSLD method described in this work is able to detect any gross errors such as incorrect calibration or movement of detector. Rectal dose in HDR brachytherapy treatments has been measured with MOSFET detectors.[56,57] Differences as large as 26% (Ref. 56) between measured and calculated doses were observed to be due to rectal filling, while other rectal measurements[57] differed by 3% or less. Based on diode measurements of rectal dose[8] the position of the HDR applicator with respect to the rectal wall changed by as much as 2.8 mm. A dose gradient of 8%/mm is common, see Table III, so changes in rectal position[7] can explain 26% differences between measured and calculated dose.

Radiochromic film and TLDs have been used to measure the skin surface dose for APBI.[58,59] The measured dose has been reported to be 9%–14% below the calculated dose. This systematic difference in dose is hypothesized to be an instance of the build-down effect. It is well known[60–62] that there is a build-down phenomenon when scatter material is removed from the side of a dose point that is distal to the source of radiation, such as at the skin surface.[63,64] This is exactly what occurs when a Nanodot is placed on the skin surface of the breast in a HDR treatment. This phenomenon is demonstrated in the experiment of Fig. 12 and it is shown that the difference in TG-43 calculated to measured dose vanishes if adequate scatter material is placed above the Nanodot. This build-down in dose is not seen in the dose calculation in Fig. 12 because the TG-43 algorithm presumes an infinite extent of water; the planning system does not properly model the dose at the skin surface. The measured skin dose in Fig. 12 is 14% below and in Table IV is 10%–17% below the TG-43 calculated dose. The Acuros algorithm as shown in Fig. 12 and Table IV correctly calculates the skin dose. The correctness of the Acuros algorithm under these conditions has been shown earlier[52,65] by comparison to Monte Carlo calculations.

The measured and TG-43 calculated doses are in agreement within experimental uncertainty as shown in Fig. 13 for various distances from the vaginal cylinder. The TG-43 calculated dose is accurate because the build-up material is 7.5 cm thick or greater for all of the detector positions. Based on the data in Fig. 12 this is adequate buildup for the TG-43 calculation algorithm to be accurate.

Another change that occurs between calibration conditions and *in vivo* measurements conditions is elevation in temperature on or in a patient. This is not a concern for OSLDs measurements since it has been shown[26] that there is no change in detector sensitivity with normal human body temperature.

VI. CONCLUSIONS

In our clinic we have successfully extended the use of OSLDs to HDR *in vivo* dosimetry. For the measurements with Nanodots in an Ir-192 radiation field to be meaningful the following conclusions must be accounted for:

1. Nanodots have a dependence on the angle of incidence of radiation.
2. Have the source orthogonal to the face of the Nanodot to avoid angle and volume-averaging corrections.
3. Surface dose is calculated incorrectly due to limitations in the TG-43 treatment-planning algorithm.
4. Measurements are in agreement within calculations within measurement uncertainty when the Acuros algorithm is used.
5. Nanodots should be calibrated with Ir-192 gamma rays before every use. Suggested calibration conditions are given in Sec. III of the paper.
6. A 10% increase in OSLD sensitivity, which depends on changes in average photon energy, occurs when measurements are made at a depth of 10 versus 1 cm in water.
7. *In vivo* dose measurements can be made successfully.

ACKNOWLEDGMENTS

The authors would like to thank the Landauer Company for providing a modified reader that had a high LED-output when the LED function-test was run.

[a]Author to whom correspondence should be addressed. Electronic mail: rsharma@wmcc.org

[1]G. Leunens, J. Van Dam, A. Dutreix, and E. Van Der Shueren, "Quality assurance in radiotherapy by *in vivo* dosimetry. 1. Entrance dose measurements, a reliable procedure," Radiother. Oncol. **17**, 141–151 (1990).

[2]G. Leunens, J. Verstraete, A. Dutreix, and E. van der Schueren, "Assessment of dose inhomogeneity at target level by *in vivo* dosimetry: Can the recommended 5% accuracy in the dose delivered to the target volume be fulfilled in daily practice?," Radiother. Oncol. **25**, 242–250 (1992).

[3]M. Essers and B. J. Mijnheer, "*In vivo* dosimetry during external photon beamradiotherapy," Int. J. Radiat. Oncol., Biol., Phys. **43**, 245–249 (1999).

[4]G. J. Kutcher, L. Coia, M. Gillin, W. F. Hanson, S. Leibel, R. J. Morton, J. R. Palta, J. A. Purdy, L. E. Reinstein, G. K. Svensson, M. Weller, and L. Wingfield, "Comprehensive QA for radiation oncology: Report of AAPM Radiation Therapy Committee Task Group 40," Med. Phys. **21**, 581–618 (1994).

[5]L. E. Cartwright, N. Suchowerska, Y. Yin, J. Lambert, M. Haque, and D. R. McKenzie, "Dose mapping of the rectal wall during brachytherapy with an array of scintillation dosimeters," Med. Phys. **37**(5), 2247–2255 (2010).

[6]P. Z. Y. Liu, P. Abolfathi, and D. R. McKenzie, "Real-time scintillation array dosimetry for radiotherapy: The advantages of photomultiplier detectors," Med. Phys. **39**(4), 1688–1695 (2012).
[7]C. Waldhausl, A. Wambersie, R. Potter, and D. Georg, "*In-vivo* dosimetry for gynaecological brachytherapy: Physical and clinical considerations," Radiother. Oncol. **77**, 310–317 (2005).
[8]K. Tanderup, J. J. Christensen, J. Granfeldt, and J. C. Lindegaard, "Geometric stability of intracavitary pulsed dose rate brachytherapy monitord by *in vivo* rectal dosimetry," Radiother. Oncol. **79**, 87–93 (2006).
[9]F. H. Attix, "Integrating dosimeters," in *Introduction to Radiological Physics and Radiation Dosimetry* (John Wiley & Sons, New York, 1986), Chap. 14, pp. 395–437.
[10]J. Van Dam and G. Marinello, *ESTRO Booklet on Physics for Clinical Radiotherapy No. 1* (Garant, Leuven-Apeldoorn, 1994).
[11]L. A. DeWerd, L. J. Bartol, and S. D. Davis, "Thermoluminescence dosimetry," in *Clinical Dosimetry for Radiotherapy: AAPM Summer School*, edited by D. W. O. Rogers and J. E. Cygler (Medical Physics, Madison, WI, 2009), pp. 815–840.
[12]E. Yorke, R. Alecu, L. Ding, R. Boissoneault, D. Fontenla, A. Kalend, D. Kaurin, M. E. Masterson-McGary, G. Marinello, T. Matzen, A. Saini, J. Shi, W. Simon, T. C. Zhu, X. R. Zhu, G. Rikner, and G. Nilsson, "Diode *in vivo* dosimetry for patients receiving external beam radiation therapy," *Report of Task Group 62 of the Radiation Therapy Committee* (Medical Physics, Madison, WI, 2005).
[13]S. Tavernier, A. Gektin, B. Grinyov, and W. W. Moses, *Radiation Detectors for Medical Applications* (Springer, Dordrecht, 2005).
[14]M. Soubra, J. Cygler, and G. Mackay, "Evaluation of a dual bias dual metal–oxide–silicon semiconductor field effect transistor detector as radiation detector," Med. Phys. **21**, 567–572 (1994).
[15]J. Lambert, T. Nakano, S. Law, J. Elsey, D. R. McKenzie, and N. Suchowerska, "*In vivo* dosimeers for HDR brachytherapy: A comparison of a diamond detectors, MOSFET, TLD, and scintillation detector," Med. Phys. **34**, 1759–1765 (2007).
[16]G. Rikner and E. Grusell, "Effect of radiation damage on p-type silicon detectors," Phys. Med. Biol. **28**, 1261–1267 (1983).
[17]G. Rikner and E. Grusell, "Patient dose measurements in photon fields by means of silicon semiconductor detectors," Med. Phys. **14**, 870–873 (1987).
[18]F. Lessard, L. Archambault, M. Plamondon, P. Després, F. Therriault-Prouix, S. Beddar, and Luc Beaulieu, "Validating plastic scintillation detectors for photon dosimetry in the radiologic energy range," Med. Phys. **39**, 5308–5316 (2012).
[19]C. E. Andersen, S. K. Nielsen, S. Greilich, J. Helt-Hansen, J. C. Lindergaard, and K. Tanderup, "Characterization of fiber-coupled Al_2O_3:C luminescent dosimetry system for online *in vivo* dose verification during ^{192}Ir brachytherapy," Med. Phys. **36**, 708–718 (2009).
[20]C. E. Andersen, S. K. Nielsen, J. C. Lindegaard, and K. Tanderup, "Time-resolved *in vivo* luminescence dosimetry for on line error detection in pulsed dose-rate brachytherapy," Med. Phys. **36**, 5033–5043 (2009).
[21]G. Kertzscher, C. E. Andersen, F. A. Siebert, S. K. Nielsen, J. C. Lindegaard, and K. Tanderup, "Identifying after loading PDR and HDR brachytherapy errors using real-time fiber-coupled Al_2O_3:C dosimetry and a novel statistical error decision criterion," Radiother. Oncol. **100**, 456–462 (2011).
[22]M. S. Akselrod, V. S. Kortov, D. J. Kravetsky, and V. I. Gotlib, "High sensitivity thermoluminescent anion-defective α-Al_2O_3:C crystal detectors," Radiat. Prot. Dosim. **32**, 15–20 (1990).
[23]M. S. Akselrod, V. S. Kortov, and E. A. Goreleva, "Preparation and properties of α-Al_2O_3:C," Radiat. Prot. Dosim. **47**, 159–164 (1993).
[24]A. J. J. Bos, "High sensitivity thermoluminescence dosimetry," Nucl. Instrum. Methods Phys. Res. B **184**, 3–28 (2001).
[25]L. Bøtter-Jensen, N. Agersnap-Larsen, B. G. Markey, and S. W. S. McKeever, "Al_2O_3:C as a sensitive OSL dosimeter for rapid assessment of environmental photon dose rate," Radiat. Meas. **27**, 295–298 (1997).
[26]P. Jursinic, "Characterization of optically stimulated luminescent dosimeters, OSLDs, for clinical dosimetric measurements," Med. Phys. **34**, 4594–4604 (2007).
[27]S. D. Miller and M. K. Murphy, "Technical performance of the Luxel α-Al_2O_3:C optically stimulated luminescence dosimeter element at radiation oncology and nuclear accident dose levels," Radiat. Prot. Dosim. **123**, 435–442 (2007).
[28]V. Schembri and B. J. M. Heijmen, "Optically stimulated luminescence (OSL) of carbon-doped aluminum oxide (Al_2O_3:C) for film dosimetry radiotherapy," Med. Phys. **34**, 2113–2118 (2007).
[29]E. G. Yukihara and S. W. S. McKeever, "Optically stimulated luminescence (OSL) dosimetry in medicine," Phys. Med. Biol. **53**, R351–R379 (2008).
[30]G. O. Sawakuchi, E. Yukihara, S. W. S. McKeever, E. Benton, R. Gaza, Y. Uchihori, N. Yasuda, and H. Kitamura, "Relative optically stimulated luminsecence and thermoluminscence efficiencies of Al_2O_3:C dosimeters to heavy charged particles with energies relevant to space and radiotherapy dosimetry," J. Appl. Phys. **104**, 124903 (2008).
[31]C. S. Reft, "The energy dependence and dose response of a commercial optically stimulated luminescent detector for kilovoltage photon, megavoltage photon, and electron, proton, and carbon beams," Med. Phys. **36**, 1690–1699 (2009).
[32]E. G. Yukihara, G. Mardirossian, M. Mirzasadeghi, S. Guduru, and S. Ahmad, "Evaluation of Al_2O_3:C optically stimulated luminescence (OSL) dosimeters for passive dosimetry of high-energy photon and electron beams in radiotherapy," Med. Phys. **35**, 260–269 (2008).
[33]A. Viamonte, L. A. da Rosa, L. A. Buckley, A. Cherpak, and J. E. Cygler, "Radiotherapy dosimetry using a commercial OSL system," Med. Phys. **35**, 1261–1266 (2008).
[34]P. A. Jursinic, "Changes in optically stimulated luminescent dosimeter (OSLD) dosimetric characteristics with accumulated dose," Med. Phys. **37**, 132–140 (2010).
[35]P. A. Jursinic and C. J. Yahnke, "*In vivo* dosimetry with optically stimulated luminescent dosimeters, OSLDs, compared to diodes; the effects of buildup cap thickness and fabrication material," Med. Phys. **38**, 5432–5440 (2011).
[36]D. W. Kim, W. K. Chung, D. O. Shin, M. Yoon, U. J. Hwang, J. E. Rah, H. Jeong, S. Y. Lee, D. Shin, S. B. Lee, and S. Y. Park, "Dose response of commercially available optically stimulated luminescent detector, Al_2O_3:C for megavoltage photons and electrons," Radiat. Prot. Dosim. **145**, 1–8 (2011).
[37]J. R. Kerns, S. F. Kry, N. Sahoo, D. S. Followill, and G. S. Ibbott, "Angular dependence of the nanoDot OSL dosimeter," Med. Phys. **38**, 3955–3962 (2011).
[38]L. A. DeWerd, G. S. Ibbott, A. S. Meigooni, M. G. Mitch, M. J. Rivarda, K. E. Stump, B. R. Thomadsen, and J. L. M. Venselaar, "A dosimetric uncertainty analysis for photon-emitting brachytherapy sources: Report of AAPM Task Group No. 138 and GEC-ESTRO," Med. Phys. **38**, 782–801 (2011).
[39]F. H. Attix, "Dosimetry fundamentals," in *Introduction to Radiological Physics and Radiation Dosimetry* (John Wiley & Sons, New York, 1986), Chap. 11, pp. 264–291.
[40]P. R. Almond, P. J. Biggs, B. M. Coursey, W. F. Hanson, M. S. Huq, R. Nath, and D. W. O. Rogers, "AAPM's TG-51 protocol for clinical reference dosimetry of high-energy photon and electron beams," Med. Phys. **26**, 1847–1870 (1999).
[41]P. Jursinic, "Angular dependence of dose sensitivity of surface diodes," Med. Phys. **36**, 2165–2171 (2009).
[42]D. R. White, "Tissue substitutes in experimental radiation physics," Med. Phys. **5**, 467–479 (1978).
[43]M. J. Rivard, B. M. Coursey, L. A. DeWerd, W. F. Hanson, M. S. Huq, G. S. Ibbott, M. G. Mitch, R. Nath, and J. F. Williamson, "Update of AAPM Task Group No. 43 Report: A revised AAPM protocol for brachytherapy dose calculations," Med. Phys. **31**, 633–674 (2004).
[44]J. A. Meli, A. S. Meigooni, and N. Ravinder, "On the choice of phantom material for the dosimetry of ^{192}Ir sources," Int. J. Radiat. Oncol., Biol., Phys. **14**, 587–594 (1988).
[45]Å. C. Tedgren, E. Rouba, H. Hedtjärn, S. Olsson, and G. A. Carlsson, "Determination of absorbed dose to water around a clinical HDR 192Ir source using LiF:Mg,Ti TLDs demonstrates an LET dependence of detector response," Med. Phys. **39**, 1133–1140 (2012).
[46]P. R. Benitez, M. E. Keisch, F. Vicini, A. Stolier, T. Scroggins, A. Walker, J. White, P. Hedberg, M. Hebert, D. Arthur, V. Zannis, C. Quiet, O. Streeter, and M. Silverstein, "Five-year results: The initial clinical trial of MammoSite balloon brachytherapy for partial breast irradiation in early-stage breast cancer," Am. J. Surg. **194**, 456–462 (2007).
[47]R. Nath, L. L. Anderson, G. Luxton, K. A. Weaver, J. F. Williamson, and A. S., Meigooni, "Dosimetry of interstitial brachytherapy sources: Recommendations of the AAPM Radiation Therapy Committee Task Group 43," Med. Phys. **22**, 209–234 (1995).
[48]A. Fogliata, G. Nicolini, A. Clivio, E. Vanetti, P. Mancosu, and L. Cozzi, "Dosimetric validation of the Acuros XB advanced dose calculation

algorithm: Fundamental characterization in water," Phys. Med. Biol. **56**, 1879–1904 (2011).
[49]J. K. Mikell and F. Mourtada, "Dosimetric impact of an 192Ir brachytherapy source cable length modeled using a grid-based Boltzmann transport equation solver," Med. Phys. **37**, 4733–4743 (2010).
[50]L. Petrokokkinos, K. Zourari, E. Pantelis, A. Moutsatsos, P. Karaiskos, L. Sakelliou, I. Seimenis, E. Georgiou, and P. Papagiannis, "Dosimetric accuracy of a deterministic radiation transport based 192Ir brachytherapy treatment planning system. Part II: Monte Carlo and experimental verification of a multiple source dwell position plan employing a shielded applicator," Med. Phys. **38**, 1981–1992 (2011).
[51]J. K. Mikell, A. H. Klopp, G. M. Gonzalez, K. D. Kisling, M. J. Price, P. A. Berner, P. J. Eifel, and F. Mourtada, "Impact of heterogeneity-based dose calculation using a deterministic grid-based Boltzmann equation solver for intracavitary brachytherapy," Int J. Radiat. Oncol., Biol., Phys. **83**, e417–e422 (2012).
[52]K. Zourari, E. Pantelis, A. Moutsatsos, L. Sakelliou, E. Georgiou, P. Karaiskos, and P. Papagiannis, "Dosimetric accuracy of a deterministic radiation transport based (192)Ir brachytherapy treatment planning system. Part III. Comparison to Monte Carlo simulation in voxelized anatomical computational models," Med. Phys. **40**, 011712 (9pp.) (2013).
[53]L. Beaulieu, Å. C. Tedgren, J.-F. Carrier, S. D. Davis, F. Mourtada, M. J. Rivard, R. M. Thomson, F. Verhaegen, T. A. Wareing, and J. F. Williamson, "Report of the Task Group 186 on model-based dose calculation methods in brachytherapy beyond the TG-43 formalism: Current status and recommendations for clinical implementation," Med. Phys. **39**, 6208–6236 (2012).
[54]S. Brown, M. McLaughlin, K. Pope, K. Haile, L. Hughes, and P. Z. Israel, "Initial radiation experience evaluating early tolerance and toxicities in patients undergoing accelerated partical breast irradiation using the Contura Multi-Lumen Balloon breast brachytherapy catheter," Brachytherapy **8**, 227–233 (2009).
[55]Z. Y. Qi, X. W. Deng, S. M. Huang, J. Lu, M. Lerch, D. Cutajar, and A. Rosenfeld, "Verification of the plan dosimetry for high dose rate brachytherapy using metal-oxide-semiconductor field effect transistor detectors," Med. Phys. **34**, 2007–2013 (2007).
[56]I. S. Kwan, D. Wilkinson, D. Cutajar, M. Lerch, A. Rosenfeld, A. Howie, J. Bucci, Y. Chin, and V. L. Pervertaylo, "The effect of rectal heterogeneity on wall dose in high dose rate brachytherapy," Med. Phys. **36**, 224–232 (2009).
[57]N. Hardcastle, D. L. Cutajar, P. E. Metcalfe, M. L. F. Lerch, V. P. Perevertaylo, W. A. Tome, and A. B. Rosenfeld, "*In vivo* real-time rectal wall dosimetry for prostate radiotherapy," Phys. Med. Biol. **55**, 3859–3871 (2010).
[58]C. A. Mangold, A. Rijnders, D. Georg, E. Van Limbergen, R. Pötter, and D. Huyskens, "Quality control in interstitial brachytherapy of the breast using pulsed dose rate: Treatment planning and dose delivery with an Ir-192 afterloading system," Radiother. Oncol. **58**, 43–51 (2001).
[59]J. A. Raffi, S. D. Davis, C. G. Hammer, J. A. Micka, K. A. Kunugi, J. E. Musgrove, J. W. Winston, Jr., T. J. Ricci-Ott, and L. A. DeWerd, "Determination of exit skin dose for 192Ir intracavitary accelerated partial breast irradiation with thermoluminescent dosimeters," Med. Phys. **37**, 2693–2702 (2010).
[60]E. C. Chamberlain and N. A. Baily, "Entrance and exit absorbed dose characteristics for a 6-mev x-ray generator," Radiology **82**, 267–271 (1964).
[61]J. A. Purdy, "Buildup surface dose and exit dose measurements for a 6-MV linear accelerator," Med. Phys. **13**, 259–262 (1986).
[62]E. E. Klein and J. A. Purdy, "Entrance and exit dose regions for a Clinac-2100C," Int. J. Radiat. Oncol., Biol., Phys. **27**, 429–435 (1993).
[63]S. Raina, J. S. Avadhani, M. Oh, H. K. Malhotra, W. Jaggernauth, M. R. Kuettel, and M. B. Podgorsak, "Quantifying IOHDR brachytherapy underdosage resulting from an incomplete scatter environment," Int. J. Radiat. Oncol., Biol., Phys. **61**, 1582–1586 (2005).
[64]A. Kelly, N. Hardcastle, P. Metcalfe, D. Cutajar, A. Quinn, K. Foo, M. Cardoso, S. Barlin, and A. Rosenfeld, "Surface dosimetry for breast radiotherapy in the presence of immobilization cast material," Phys. Med. Biol. **56**, 1001–1013 (2011).
[65]E. Pantelis, P. Papagiannis, P. Karaiskos, A. Angelopoulos, G. Angelopoulos, D. Baltas, N. Zamboglou, and L. Sakelliou, "The effect of finite patient dimensions and tissue inhomogeneities on dosimetric planning of ^{192}Ir HDR breast brachytherapy: A Monte Carlo dose verification study," Int. J. Radiat. Oncol., Biol., Phys. **61**, 1596–1602 (2005).